Electronic Supplementary Material (ESI) for Nanoscale.

CeO_{2-x} Nanorods with Intrinsic Urease-Like Activity

K. Korschelt,[a] R. Schwidetzky,[a] F. Pfitzner,[a] J. Strugatchi,[a] C. Schilling,[b] M. von der Au,[c] K. Kirchhoff,[d] M. Panthöfer,[a] I. Lieberwirth,[d] M. N. Tahir,[e] C. Hess,[b] B. Meermann,[c] W. Tremel[a]*

[a] Institut für Anorganische Chemie und Analytische Chemie, Johannes Gutenberg-Universität, Duesbergweg 10-14, D-55128 Mainz, Germany. Homepage: http://www.ak-tremel.chemie.uni-mainz.de/

[b] Eduard-Zintl-Institut Institut für Physikalische Chemie, Technische Universität Darmstadt, Alarich-Weiss-Str. 8 D-64287 Darmstadt, Germany

[c] Federal Institute of Hydrology, Departement G2 Aquatic Chemistry, Am Mainzer Tor 1, D-56068 Koblenz, Germany

[d] Max Planck Institute for Polymer Research, Ackermannweg 10, D-55128 Mainz, Germany

[e] King Fahd University of Petroleum and Minerals, Kingdom of Saudi Arabia.

* *Corresponding Author: tremel@uni-mainz.de*

Figures

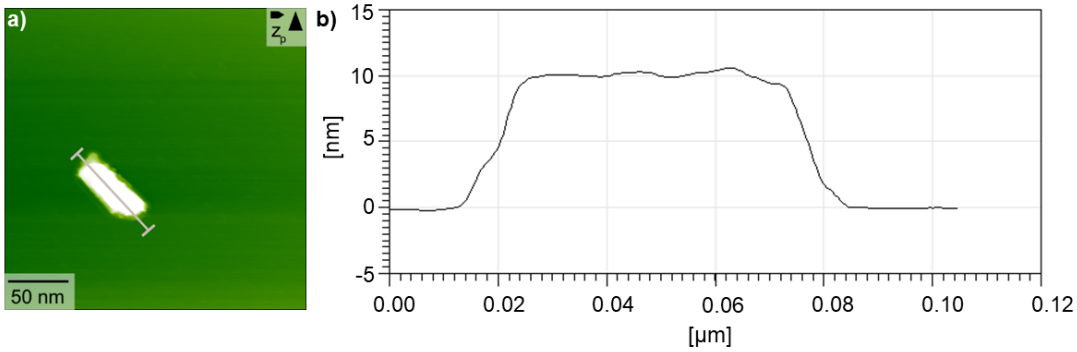

Fig. S1. AFM image of CeO_{2-x} NRs showing a height of approx. 9-11 nm.

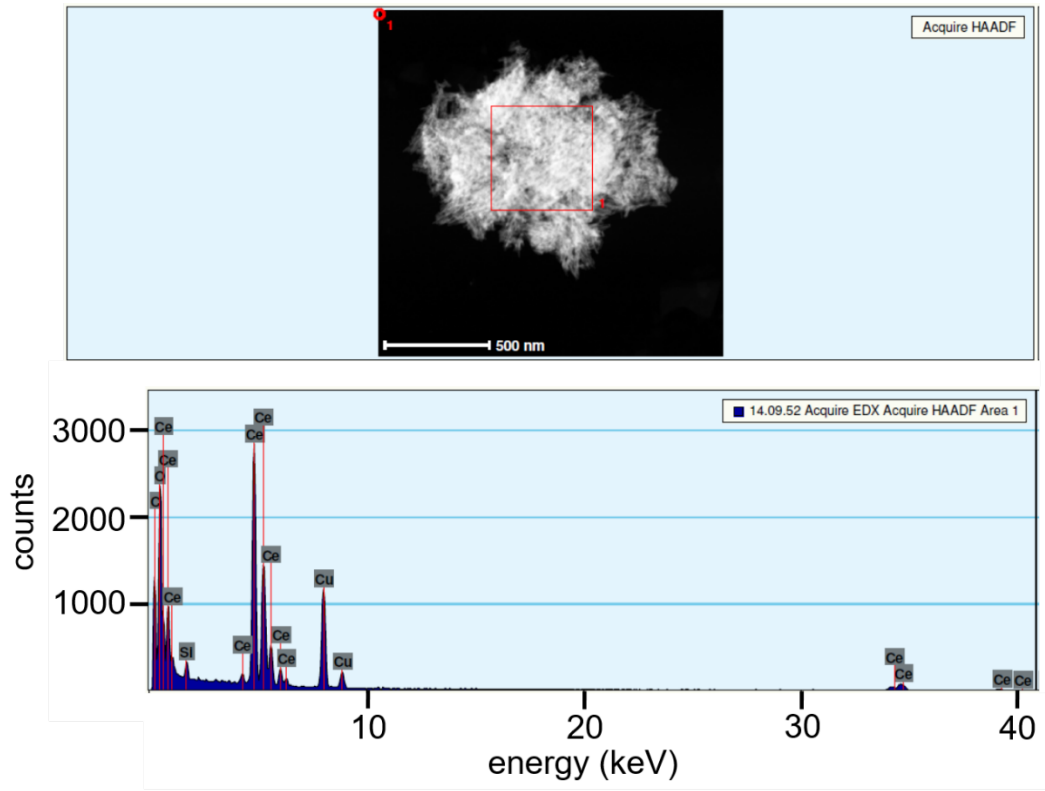

Fig. S2. EDX spectrum of CeO_{2-x} NRs.

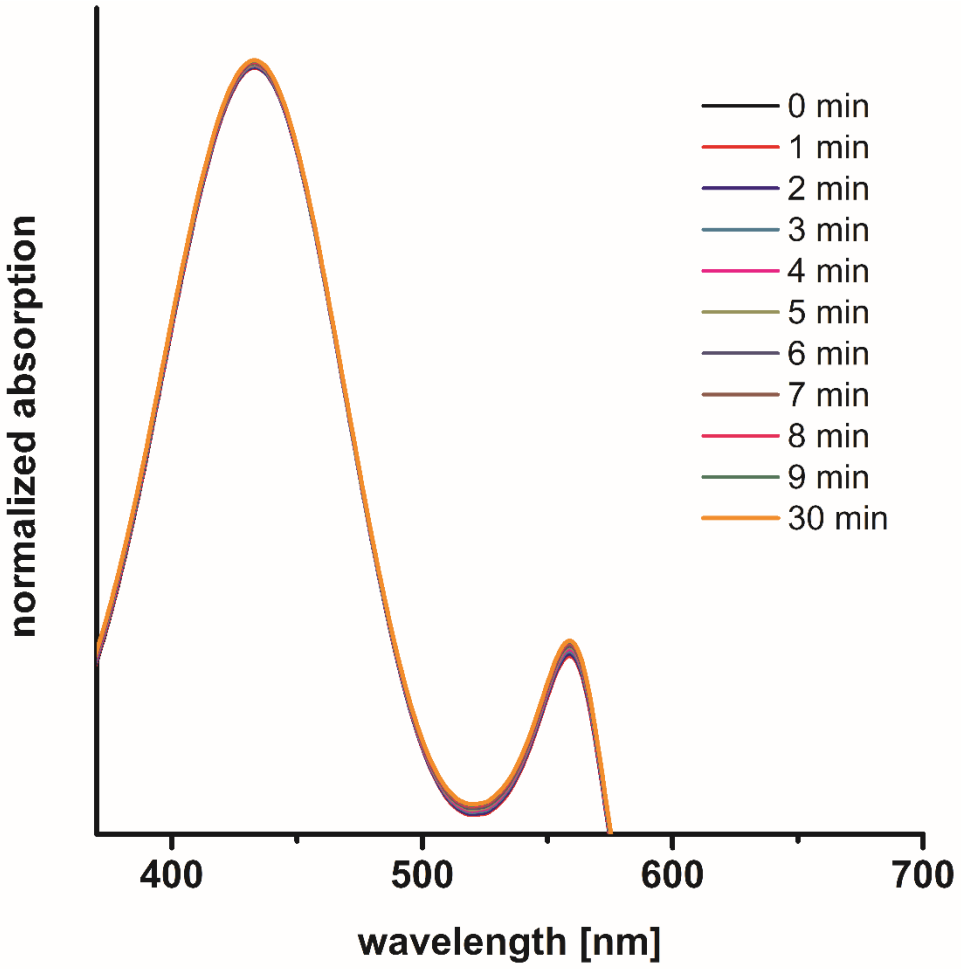

Fig. S3. Kinetic absorption scan of a phosphate buffered solution containing phenol red and urea without enzyme mimic show no significant change of absorptions at 434 nm and 560 nm.

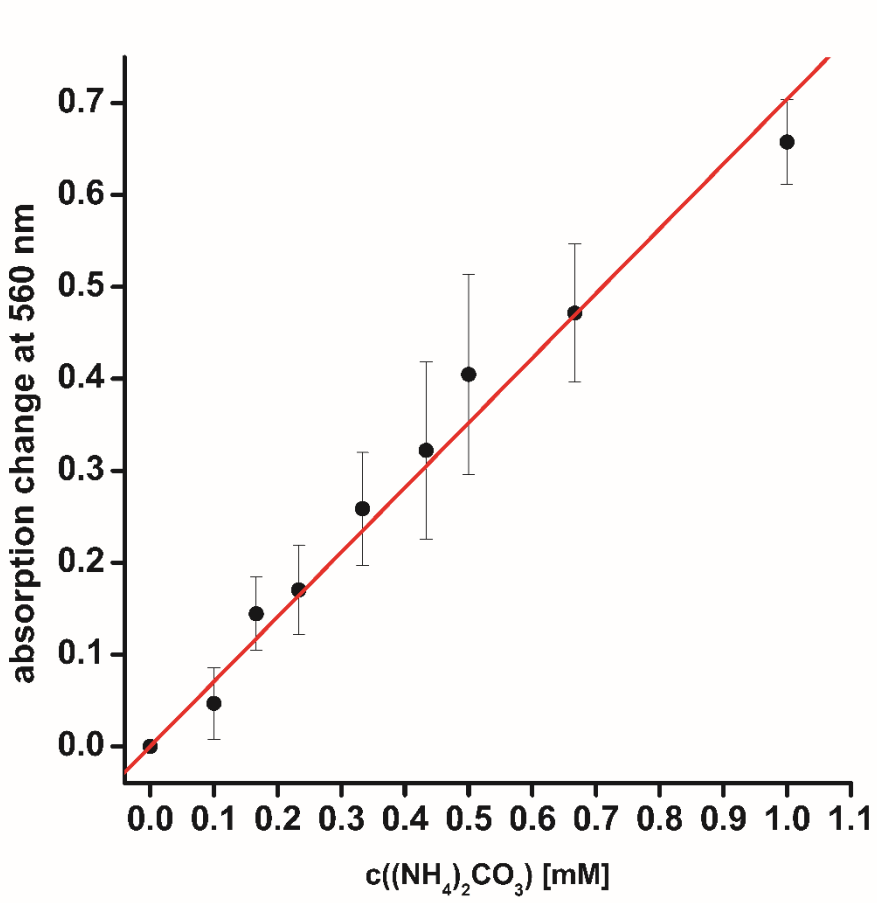

Fig. S4. Calibration conducted with 0.1 M ammonium carbonate ($(NH_4)_2CO_3$) solution enables the combination of formed or added amount of ammonium carbonate and the resulting absorption change at 560 nm. Calibrations were done prior to each measurement.

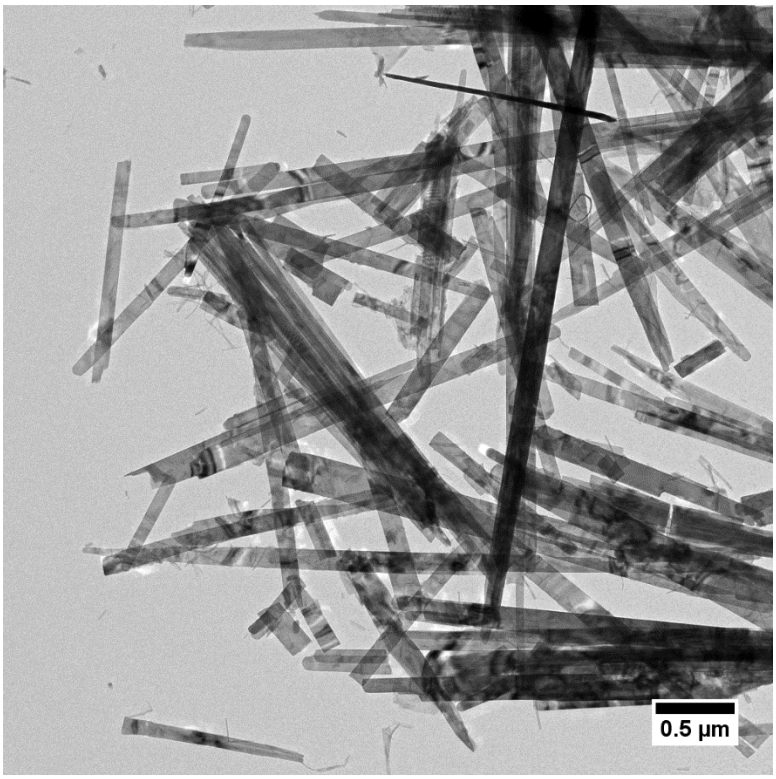

Fig. S5. Representative TEM image of MoO_{3-x} nanobelts.

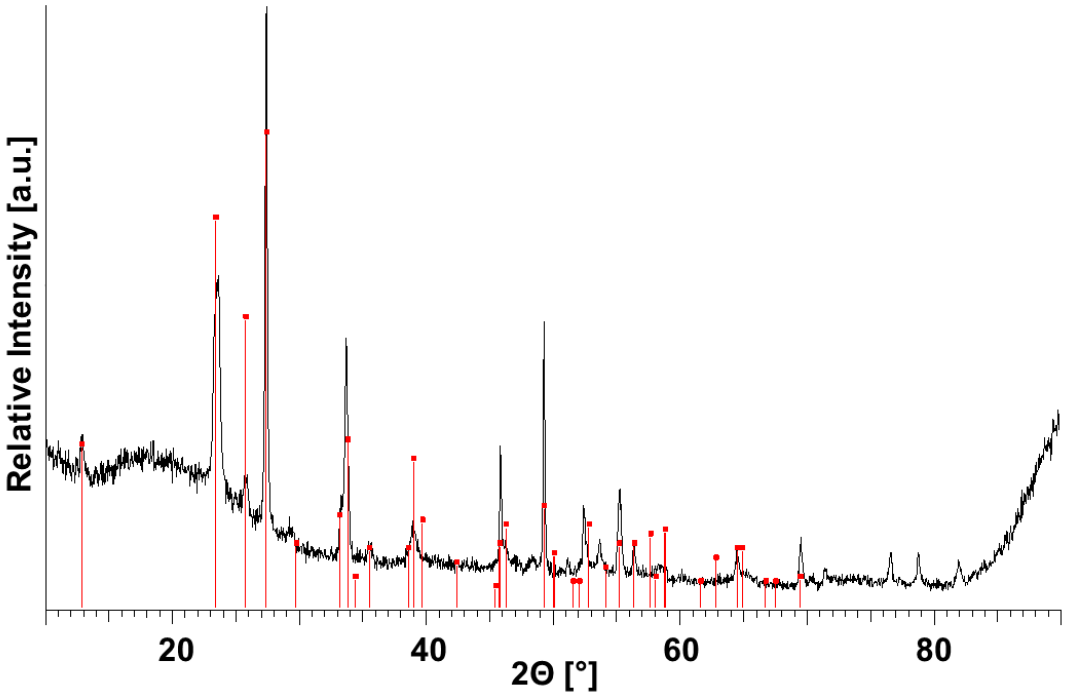

Fig. S6. Powder diffractogram of MoO_{3-x} nanobelts and calculated reflection positions of MoO_3 (red).

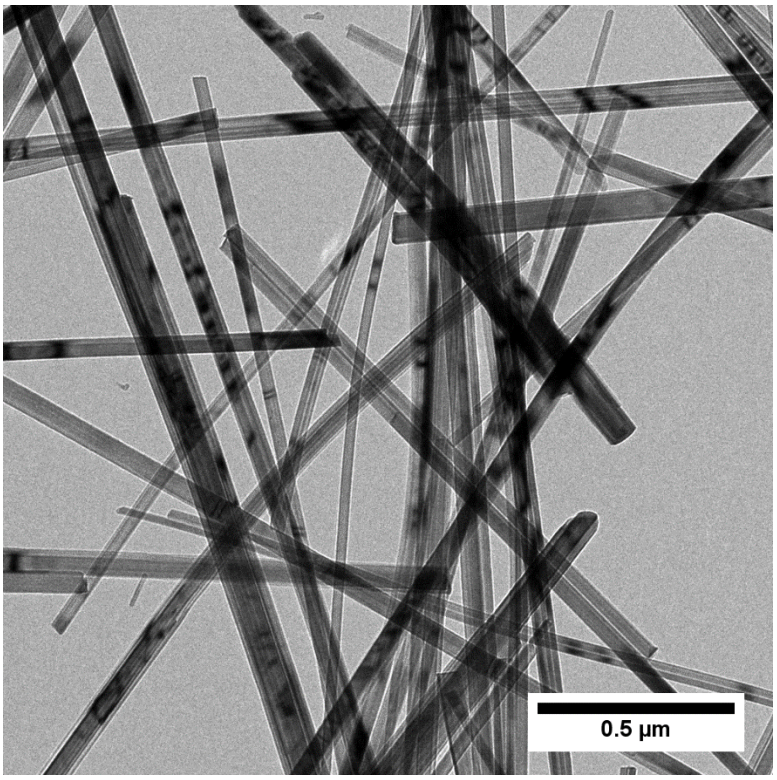

Fig. S7. Representative TEM image of V_2O_5 nanowires.

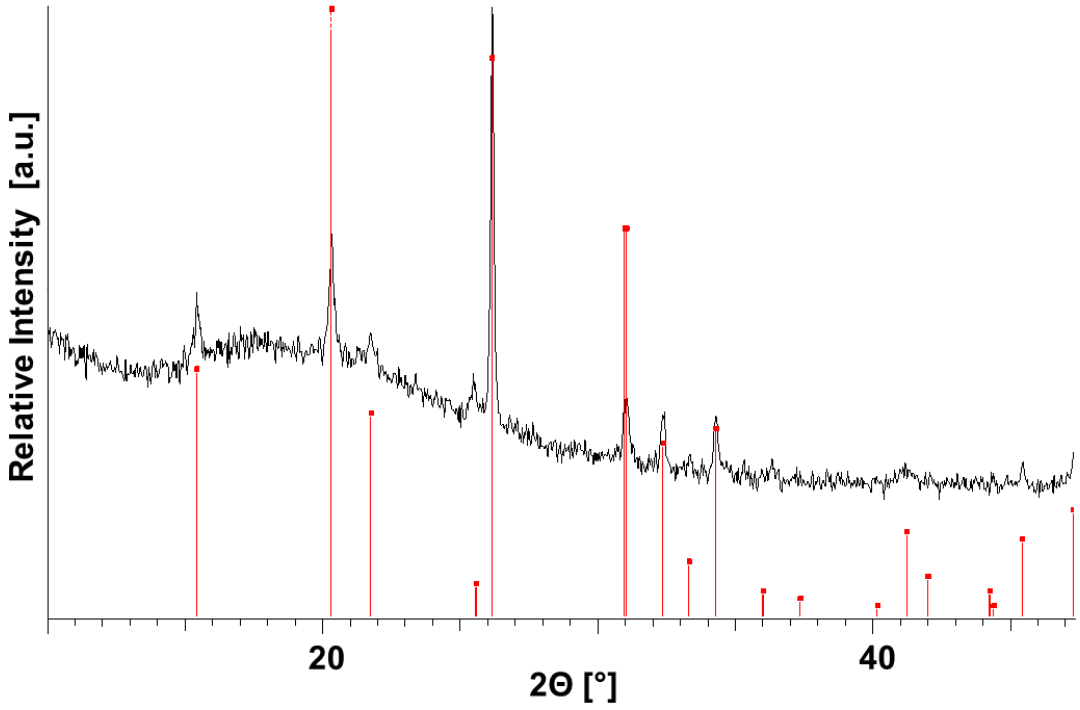

Fig. S8. Powder diffractogram of V_2O_5 nanowires.

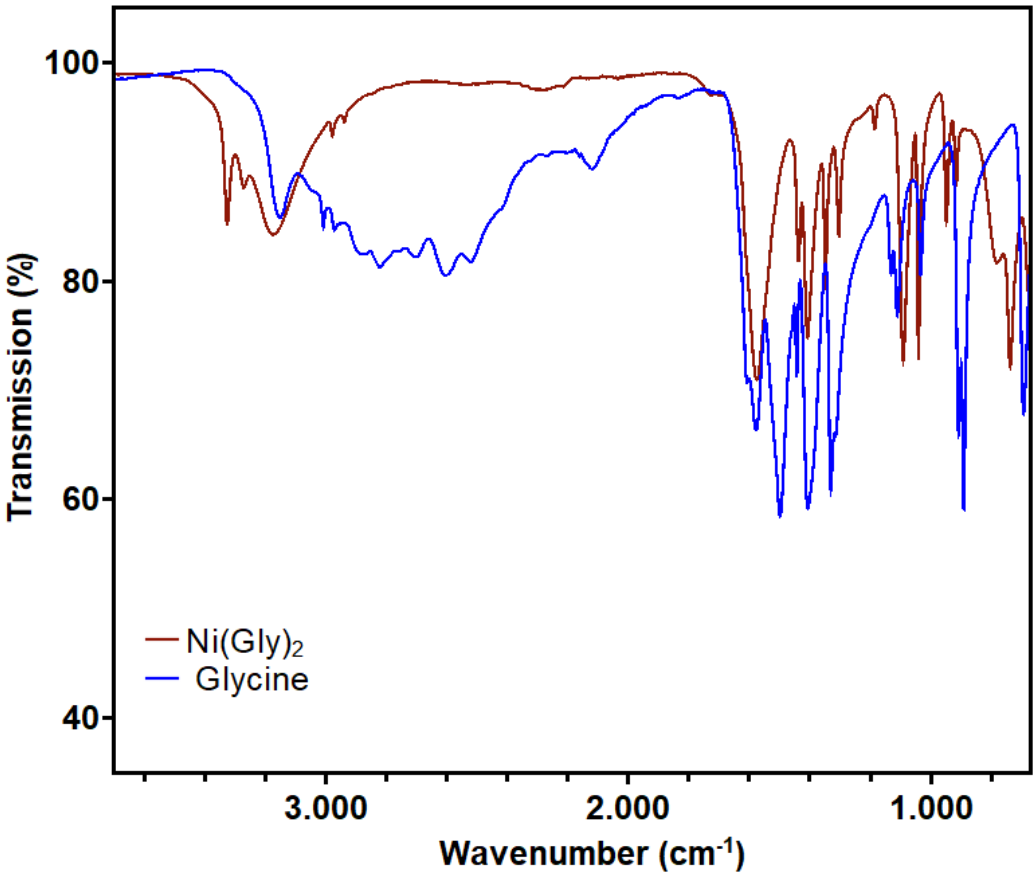

Fig. S9. IR spectra of the $Ni(Gly)_2$ complex and glycine.

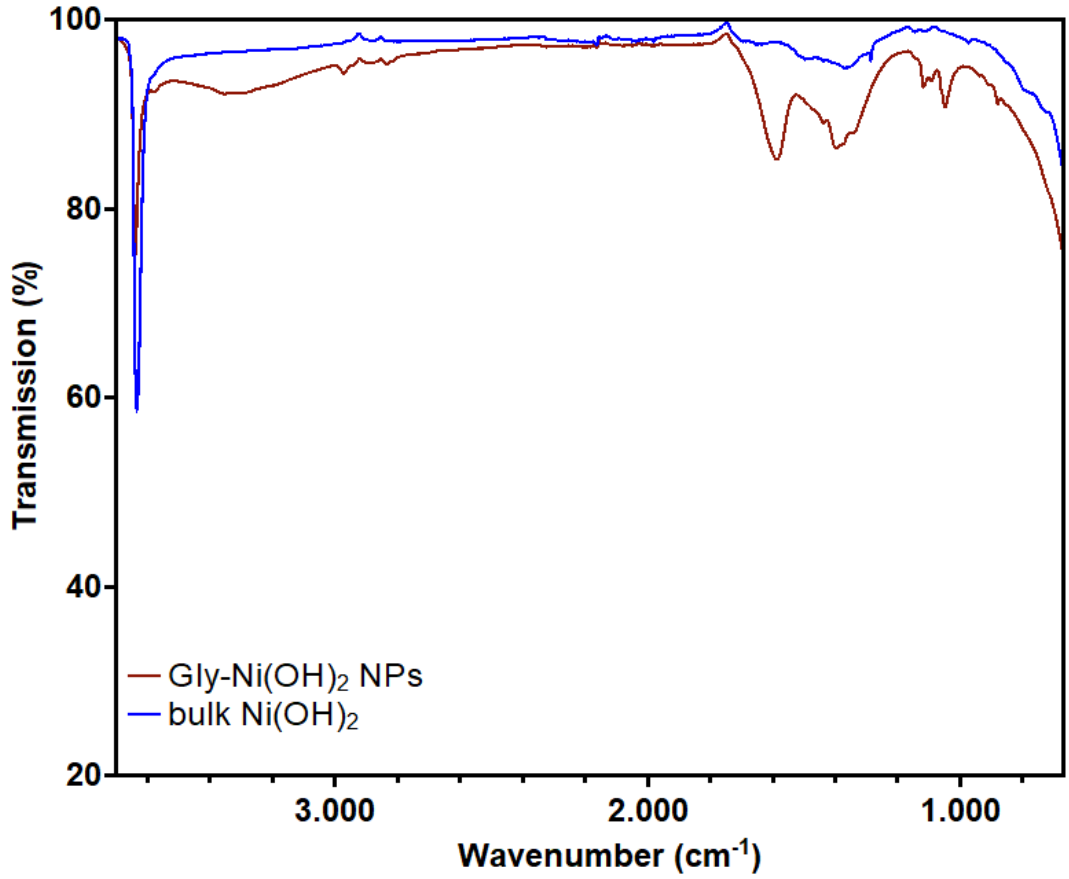

Fig. S10. IR spectra of Gly-Ni(OH)$_2$ NPs and bulk Ni(OH)$_2$.

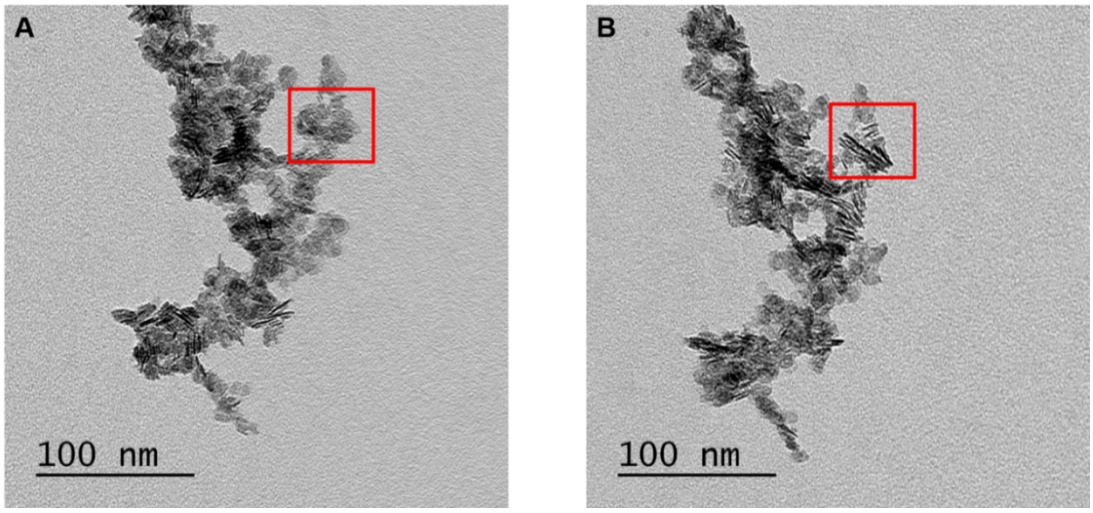

Fig. S11. TEM images of Gly-Ni(OH)$_2$ NPs. TEM images show the formation of Ni(OH)$_2$ nanosheets with a diameter of approx. (10.62 ± 1.29) nm. The TEM images where tilted - 40° (A) and + 40° (B) to demonstrate the sheet structure.

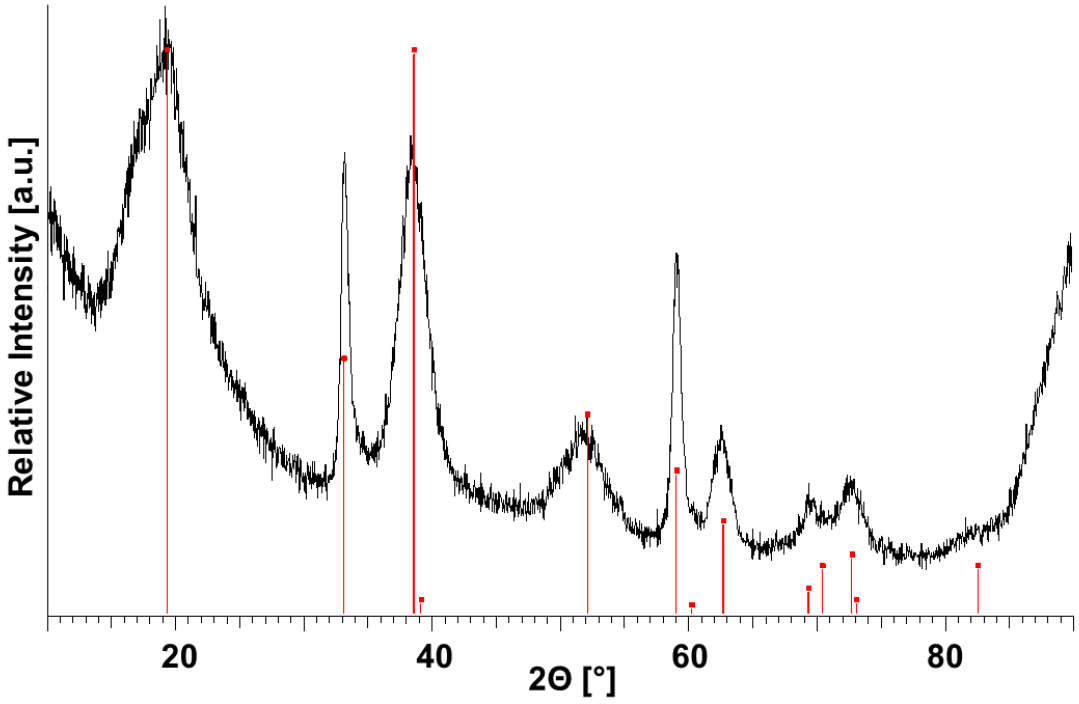

Fig. S12. P-XRD measurement of Gly-Ni(OH)$_2$ NPs. Measured pattern (black) and reflection positions of theoprastite (red). The sheet structure seen in the TEM images of Gly-Ni(OH)$_2$ NPs is demonstrated by the broadened reflections (flat plane), and sharp reflections (thickness of the as-synthesized NPs).

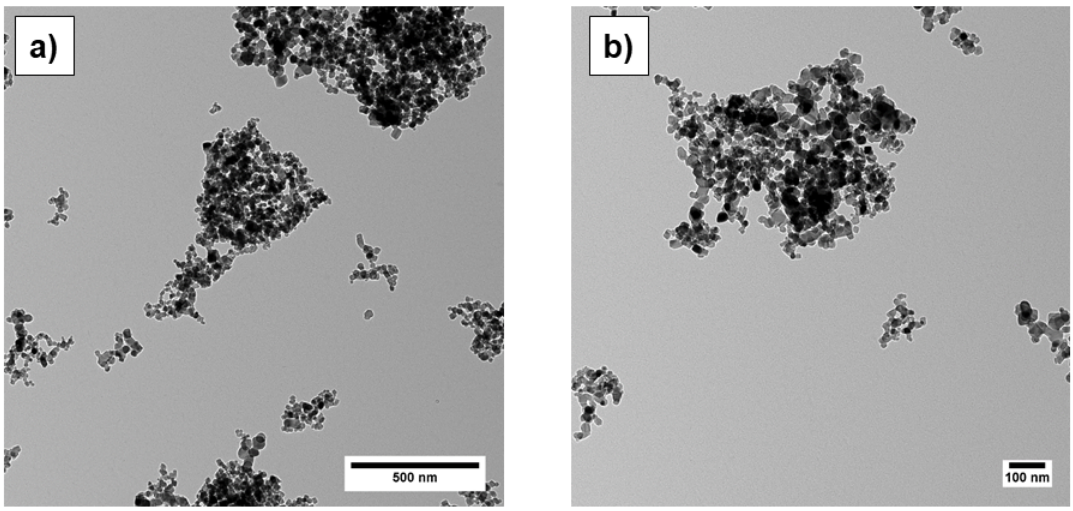

Fig. S13. TEM images of commercially available TiO_2 nanoparticles.

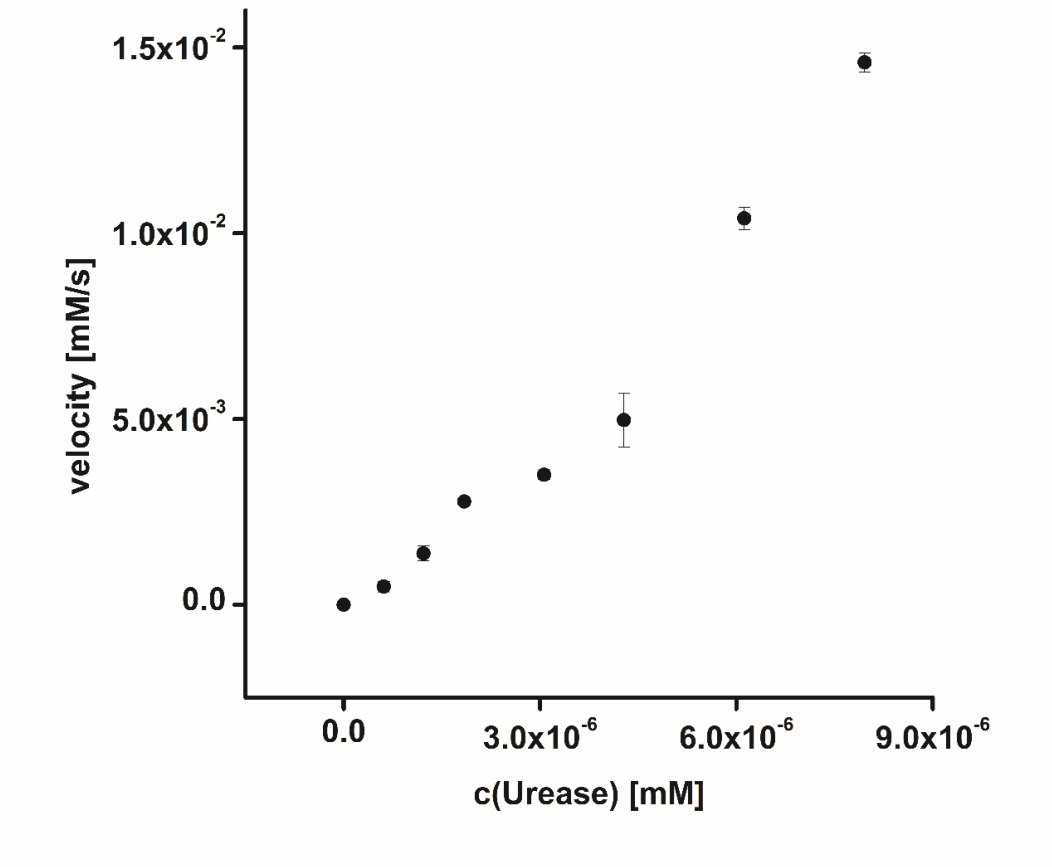

Fig. S14. Variation of the concentration of native urease show that increasing enzyme concentrations lead to higher urea degradation. Error bars are calculated from three repeats.

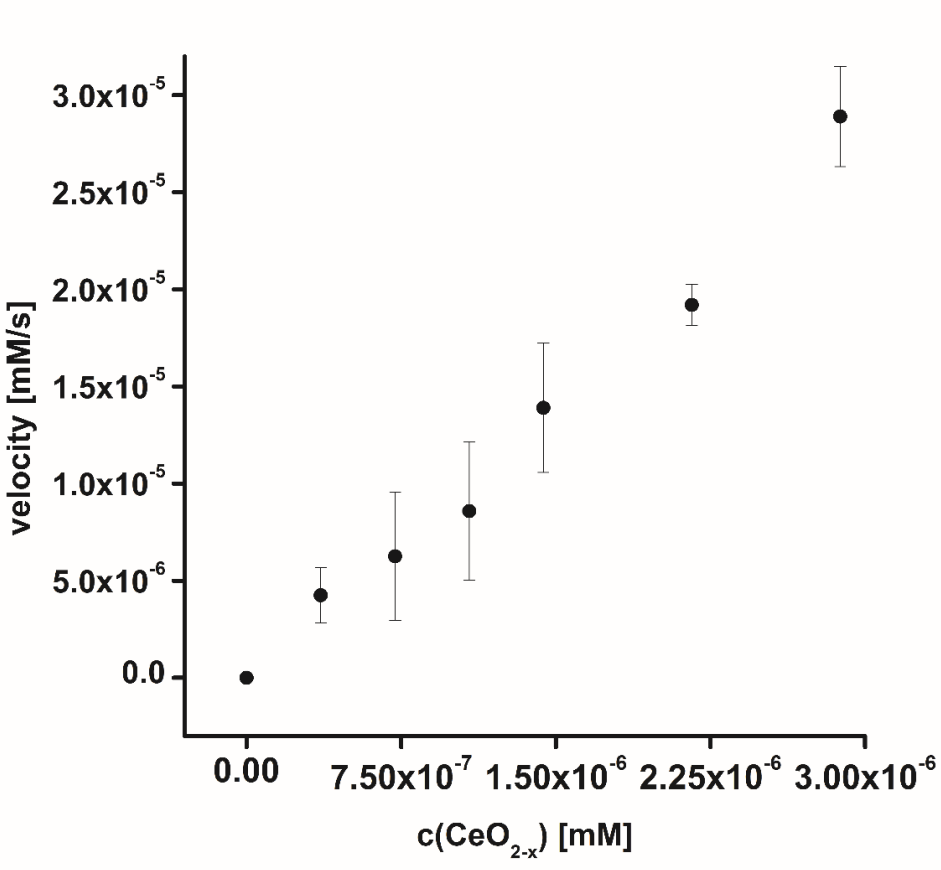

Fig. S15. Variation of CeO_{2-x} NR concentration shows the dependency of catalyst concentration to substrate degradation. Increasing amounts of nanoparticles lead to an increase of urea decomposition. Error bars are calculated from three repeats.

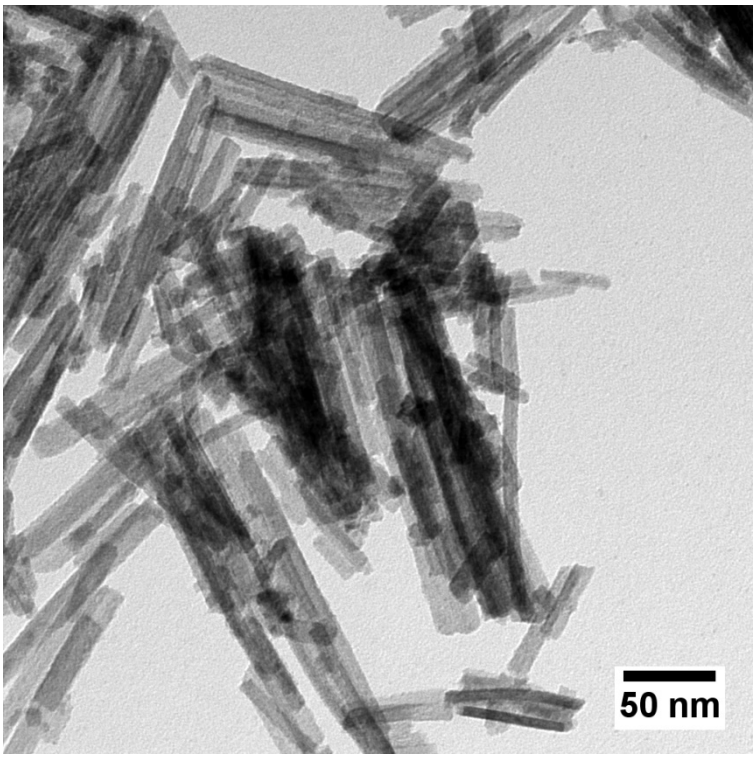

Fig. S16. TEM image of $Ce_{0.6}La_{0.4}O_{1.80-x}$ NRs**.**

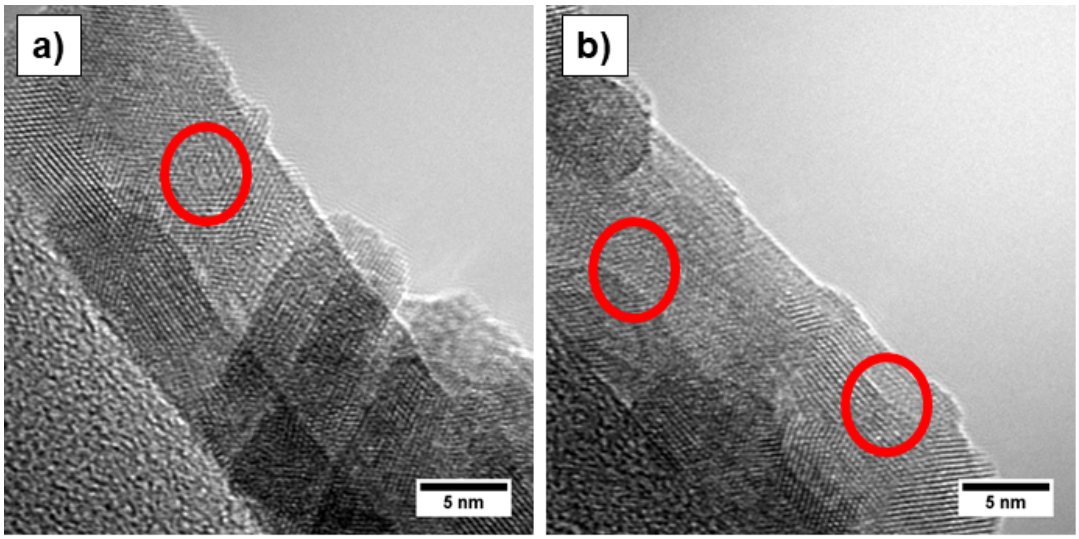

Fig. S17. HR-TEM images of $Ce_{0.6}La_{0.4}O_{1.80-x}$ NRs. The images show the presence of surface defects, similar to the NR sample with a composition of $Ce_{0.9}La_{0.1}O_{1.95-x}$. The d spacings of 0.3 nm correspond to the (111) plane of CeO_2.

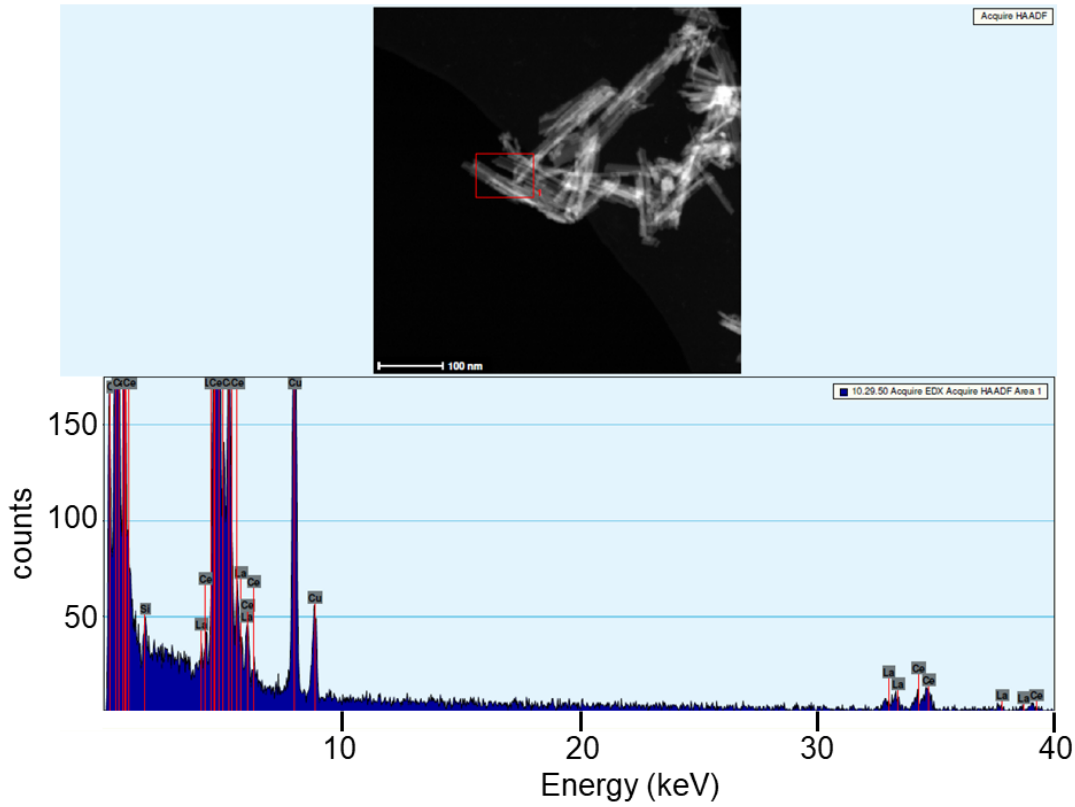

Fig. S18. EDX spectrum of $Ce_{0.6}La_{0.4}O_{1.80-x}$ NRs. The spectrum shows the presence of La and Ce in the sample, and no further metal impurities.

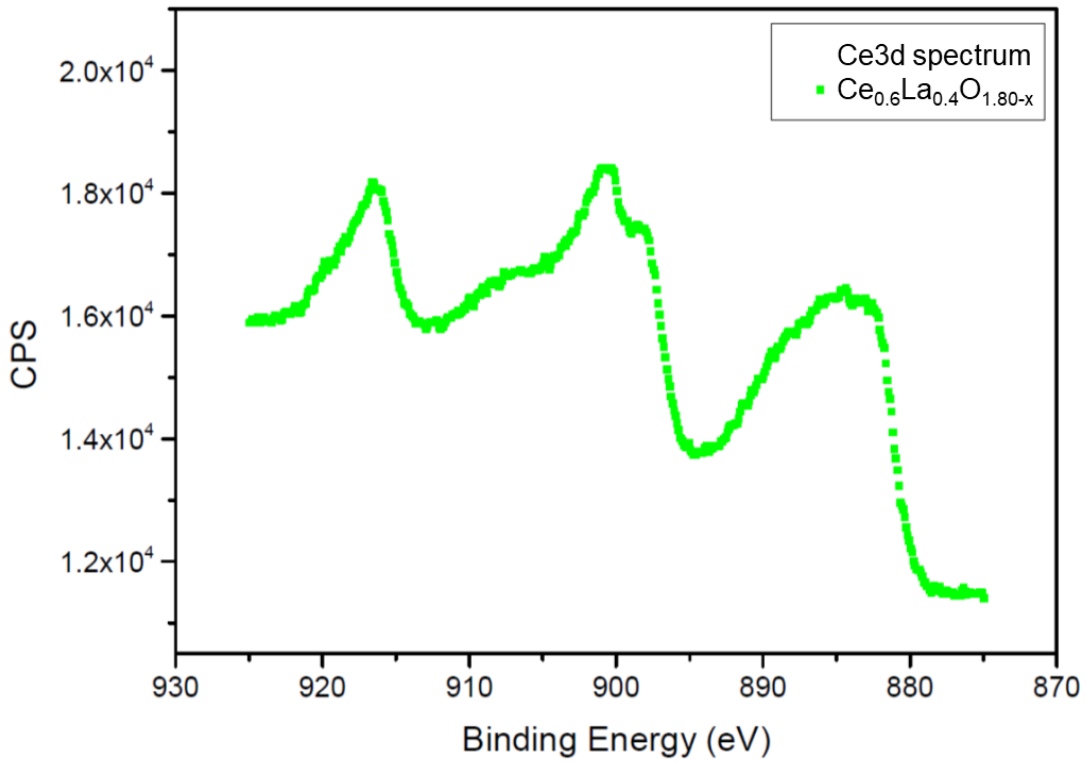

Fig. S19. XPS spectrum of $Ce_{0.6}La_{0.4}O_{1.80-x}$ NRs. The spectrum shows a higher amount of Ce^{3+} compared to the un-doped CeO_{2-x} and to the $Ce_{0.9}La_{0.1}O_{1.95-x}$ CeO_{2-x} nanorods. A $Ce^{3+}/(Ce^{3+}+Ce^{4+})$ ratio of 26.9 was extracted from the spectra.

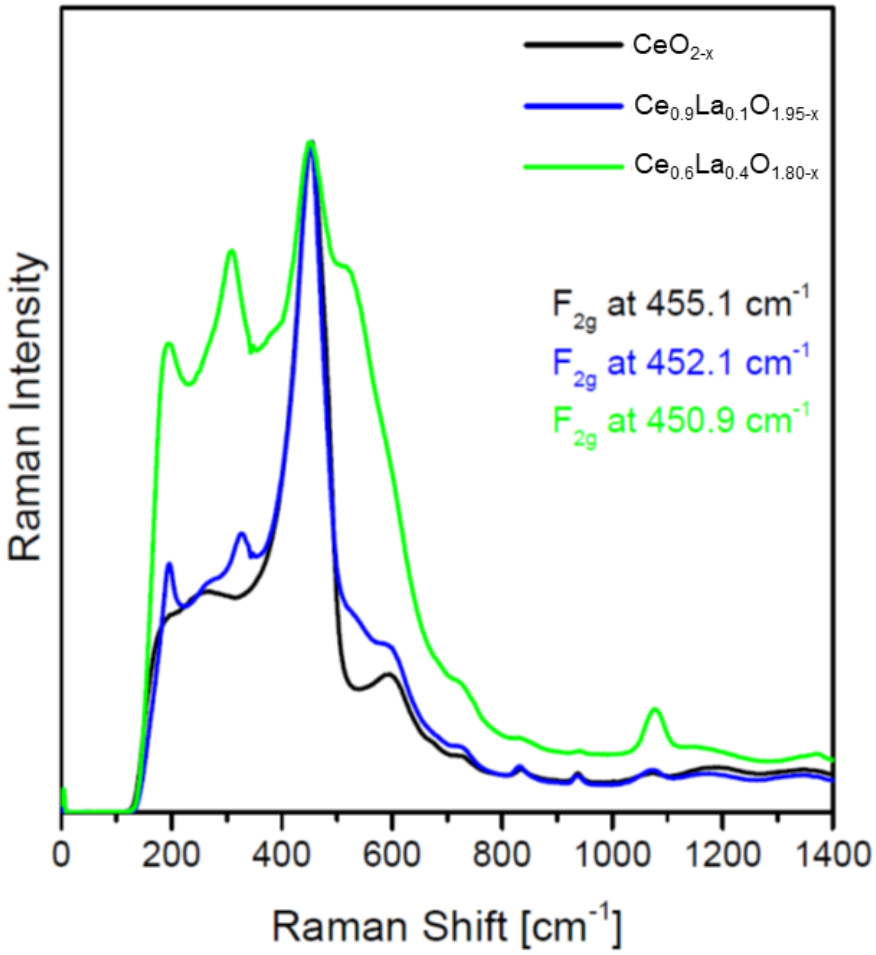

Fig. S20. Raman spectra of CeO_{2-x}, $Ce_{0.9}La_{0.1}O_{1.95-x}$ and $Ce_{0.6}La_{0.4}O_{1.80-x}$ NRs.

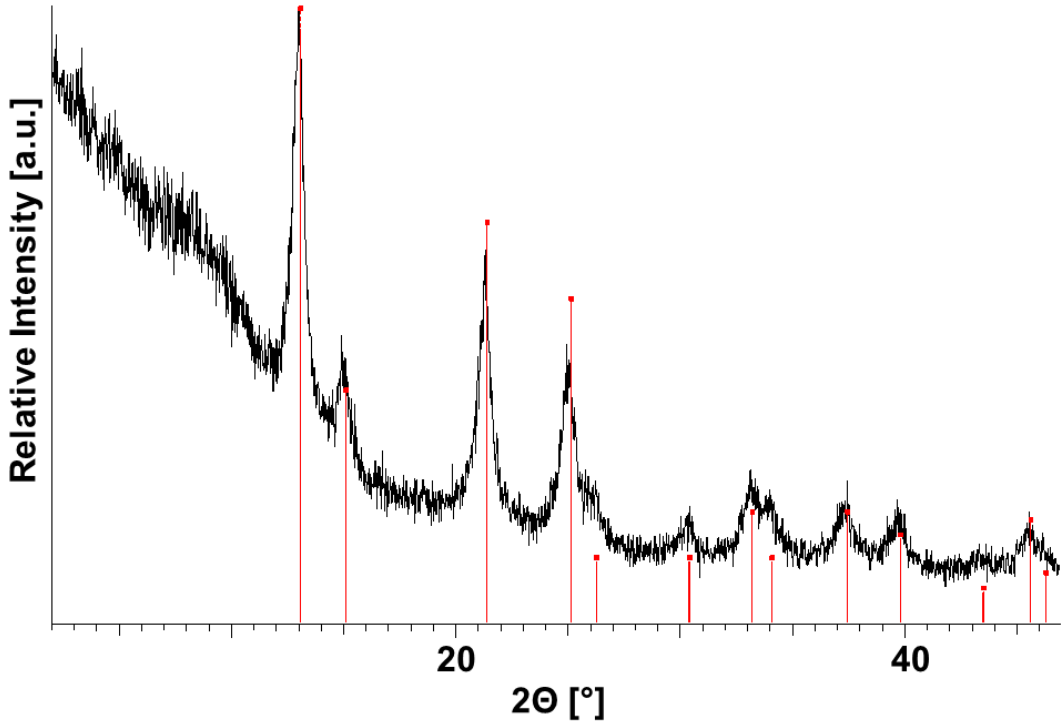

Fig. S21. P-XRD measurement of $Ce_{0.6}La_{0.4}O_{1.80-x}$ NRs. The reflection positions of the measured pattern (black) are shifted to higher angles compared to the control pattern of cerianite (red). The results are in harmony with the difractogramm measured for $Ce_{0.9}La_{0.1}O_{1.95-x}$, where a detailed Rietveld refinement was carried out.

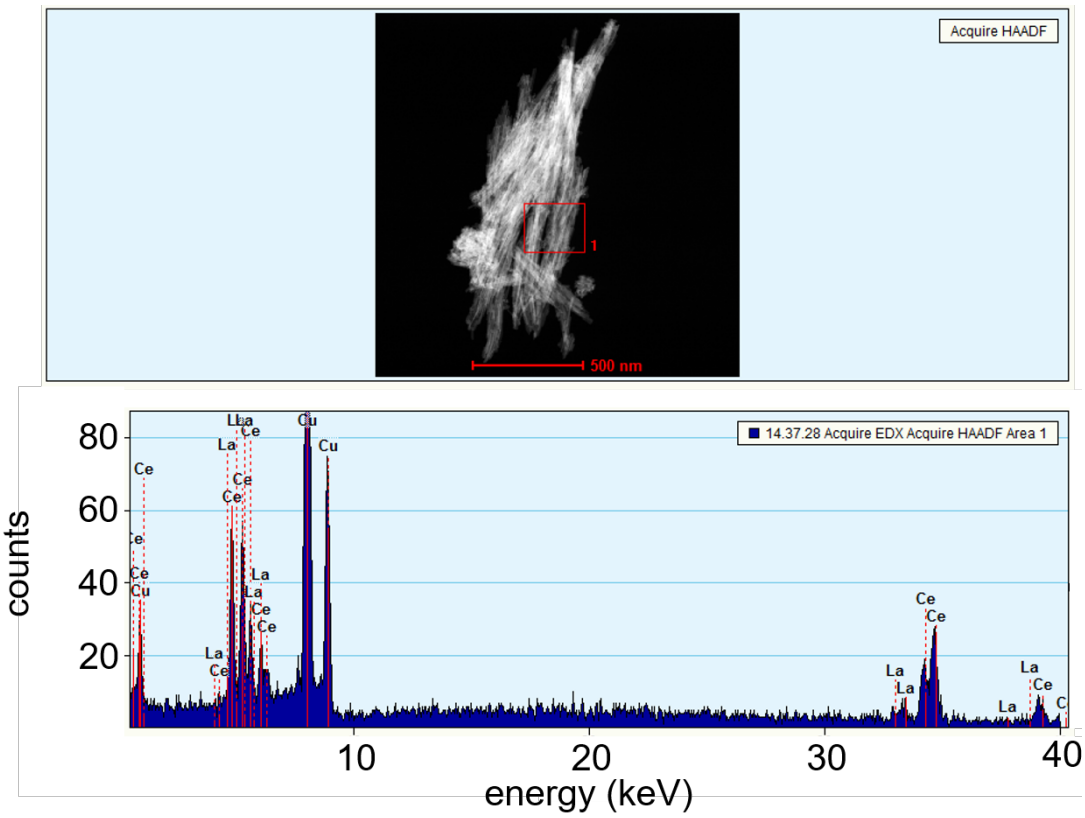

Fig. S22. EDX measurement of $Ce_{0.9}La_{0.1}O_{1.95-x}$ NRs. The analysis revealed the presence of La in the sample. The results are in harmony with the results of the XPS and ICP-MS analysis.

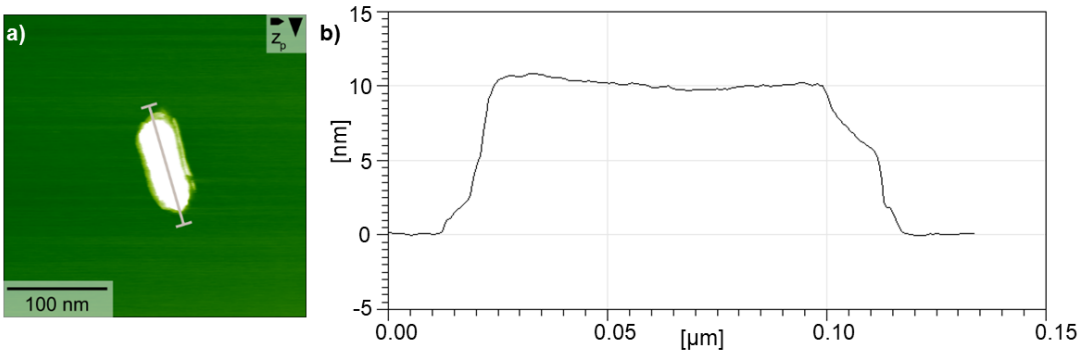

Fig. S23. AFM image of $Ce_{0.9}La_{0.1}O_{1.95-x}$ NRs show a height of approx. 9-11 nm.

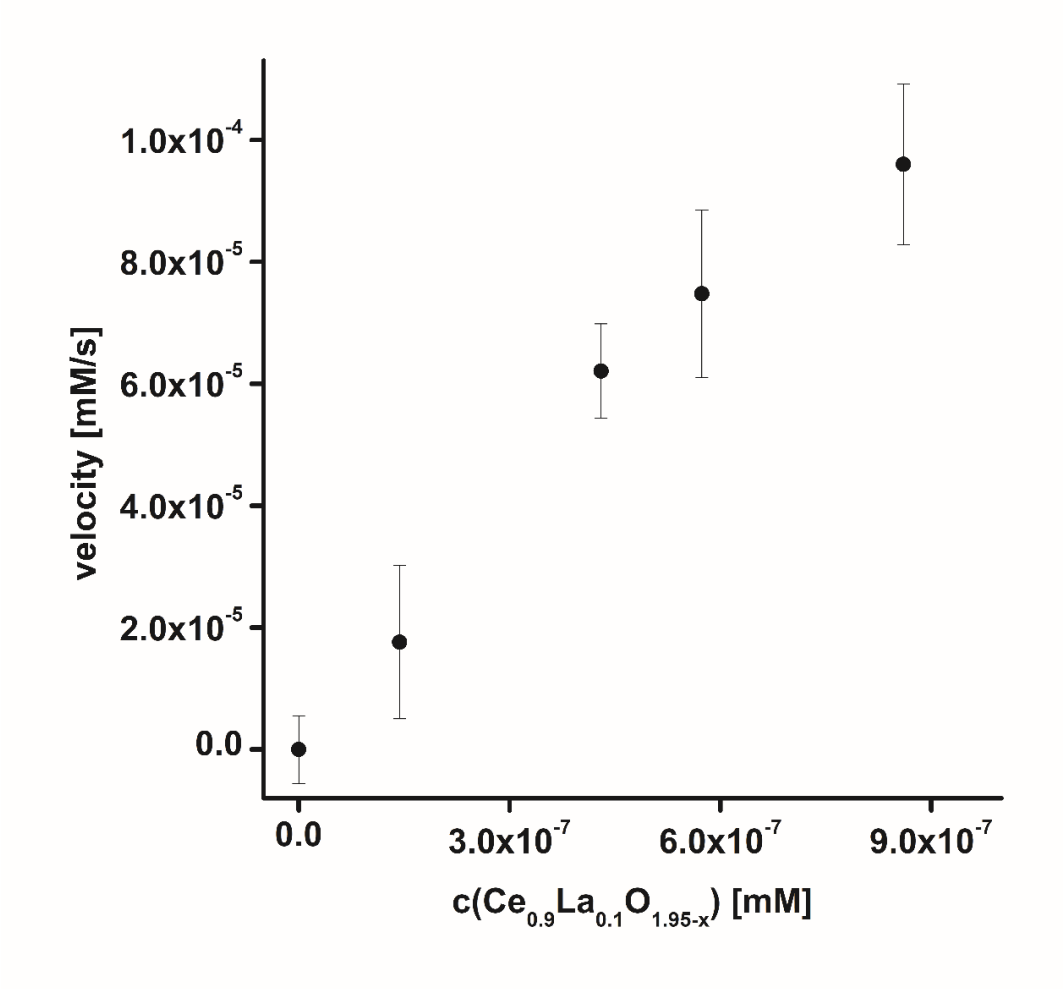

Fig. S24. Variation of the $Ce_{0.9}La_{0.1}O_{1.95-x}$ NR concentration shows an increase of urea degradation with increasing particle concentration.

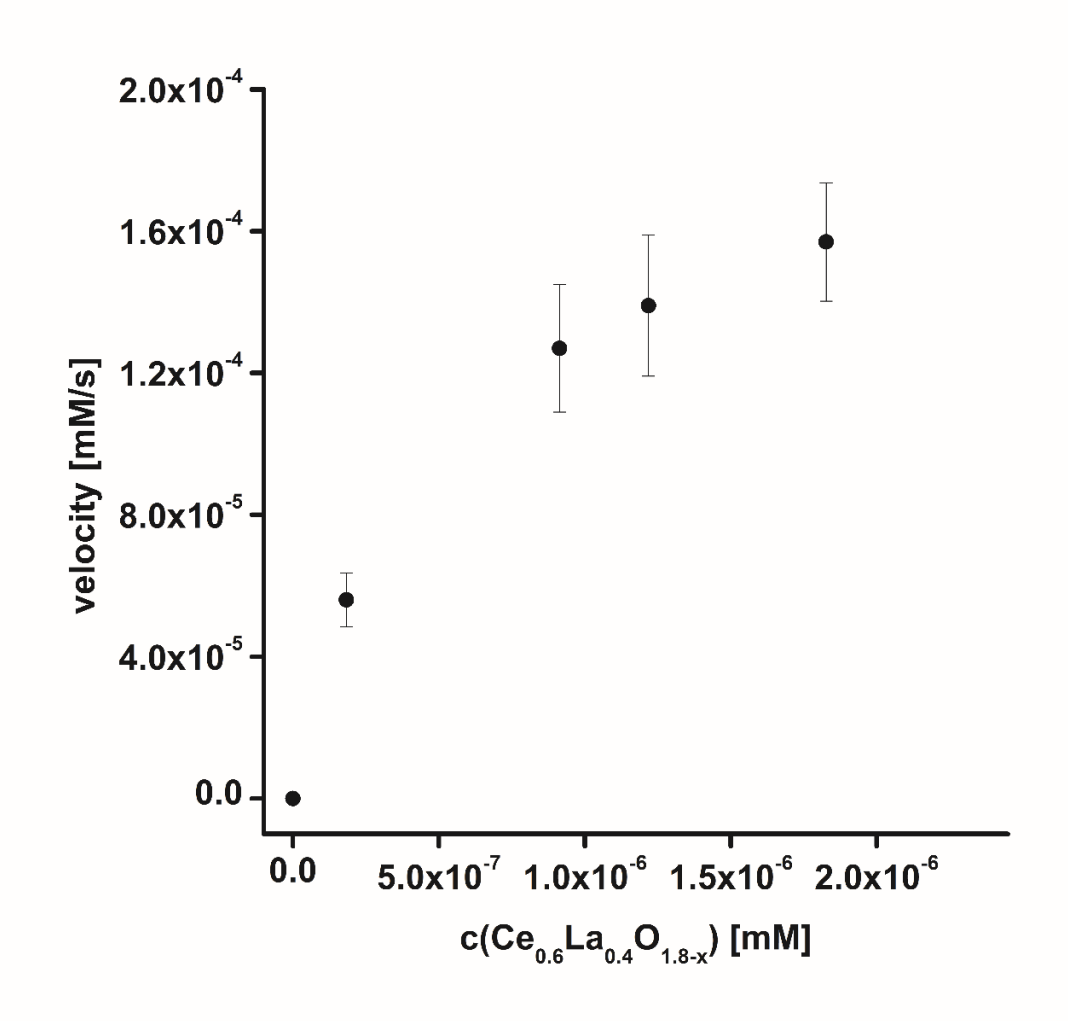

Fig. S25. Variation of the $Ce_{0.6}La_{0.4}O_{1.8-x}$ NR concentration shows an increase of urea degradation with increasing particle concentration.

Tables

Tab. S1. Data obtained from Rietveld refinements.

	CeO_{2-x}	$Ce_{0.9}La_{0.1}O_{1.95-x}$
Device	STOE Stadi P, Mo Kα1, Mythen 1K, transmission geometry	
Sample Prep	Powder between two vinyl acetate foils (15µm)	
Measruement conditions	$1.5 < 2\Theta/° < 70.83$, resolution $\Delta\Theta = 0.015°$ step scan, step size 1°, step time Δt =180 s	
Background	Adapted	
r_{wp}	4.95	5.82
Gof	2.09	1.86
Space group	*Fm*-3*m*	
Lattice Parameter / Å	a = 5.4071(6)	a = 5.9685(2)
Crystallite size / nm	6.8(3)	5.9(8)

Tab. S2. Surface composition from XPS analysis.

Compound	C at%	O at%	Ce at%	La at%	O/(Ce + La)
CeO_{2-x}	9.9	57.0	33.1	-	1.72
$Ce_{0.9}La_{0.1}O_{1.95-x}$	8.5	55.9	30.7	4.9	1.57
$Ce_{0.6}La_{0.4}O_{1.80-x}$	9.6	55.7	17.4	17.3	1.60

Tab. S3. Leaching of Ce of CeO_{2-x}NRs in MilliQ water. Data are corrected against standard, but not blank corrected due to low blank values.

sample	c(Ce) [µg L^{-1}]	SD [µg L^{-1}]
blank (1)	0.04	0.005
blank (2)	0.03	0.003
blank (3)	0.05	0.004
CeO_{2-x} (1)	0.4	0.1
CeO_{2-x} (3)	1.6	0.1
CeO_{2-x} (2)	0.8	0.1

Tab. S4. Leaching of Ce and La of $Ce_{0.9}La_{0.1}O_{1.95-x}$ NRs in MilliQ water. Data corrected against standard, but not blank corrected, due to low blank values.

sample	c(Ce) [µg L^{-1}]	SD [µg L^{-1}]	c(La) [µg L^{-1}]	SD [µg L^{-1}]
blank (1)	0.2	0.01	0.02	0.003
blank (2)	0.1	0.01	0.01	0.002
blank (3)	0.1	0.01	0.01	0.002
$Ce_{0.9}La_{0.1}O_{1.95-x}$ (1)	4.8	0.2	5.4	0.2
$Ce_{0.9}La_{0.1}O_{1.95-x}$ (2)	3.1	0.2	6.3	0.3
$Ce_{0.9}La_{0.1}O_{1.95-x}$ (3)	5.0	0.2	5.9	0.2

Tab. S5. Leaching of Ce of CeO_{2-x} NRs in 2.94 M urea solution. Data corrected against standard, but not blank corrected due to low blank values.

sample	c(Ce) [µg L^{-1}]	SD [µg L^{-1}]
blank (1)	0.5	0.02
blank (2)	0.6	0.03
blank (3)	0.4	0.02
CeO_{2-x} (1)	12.3	0.7
CeO_{2-x} (2)	8.1	0.3
CeO_{2-x} (3)	5.9	0.3

Tab. S6. Leaching of Ce and La of $Ce_{0.9}La_{0.1}O_{1.95-x}$ NRs in 2.94 M urea solution. Data corrected against standard, but not blank corrected due to low blank values.

sample	c(Ce) [µg L^{-1}]	SD [µg L^{-1}]	c(La) [µg L^{-1}]	SD [µg L^{-1}]
blank (1)	0.5	0.02	0.01	0.001
blank (2)	0.6	0.03	0.03	0.003
blank (3)	0.4	0.02	0.01	0.000
$Ce_{0.9}La_{0.1}O_{1.95-x}$ (1)	6.2	0.2	9.4	0.2
$Ce_{0.9}La_{0.1}O_{1.95-x}$ (2)	3.3	0.2	5.2	0.1
$Ce_{0.9}La_{0.1}O_{1.95-x}$ (3)	6.7	0.4	5.5	0.2